Int. J. Electrochem. Sci., 17 **(2022)** Article Number: 220430, doi: 10.20964/2022.04.04

International Journal of
ELECTROCHEMICAL
SCIENCE
www.electrochemsci.org

Short Communication

In-Situ Synthesis of Cauliflower-like FeS_2 Grown on 3D Graphene Foam as High-performance Electrode for Na^+ Storage

Xin Wang[1,*], *Yinling Zhang*[2], *Jia Li*[1], *Hengxu Liu*[1], *Dongping Li*[1,*]

[1] School of Materials Science and Chemical Engineering, Harbin University of Science and Technology, Harbin 150080, PR China
[2] Heilongjiang Academy of Mechanical Science, Harbin 150080, PR China
[*]E-mail: wangxin0120@163.com

Received: 16 December 2021 / *Accepted:* 24 January 2022 / *Published:* 4 March 2022

Herein, samples of in-situ obtained FeS_2 were successfully grown on three dimensional (3D) graphene foam (3DGF), forming a free-standing flower bud-like and cauliflower-like structure (labelled as FeS_2 FB/3DGF and FeS_2 CF/3DGF). Both were used as anode materials for sodium-ion batteries (SIBs), which exhibited high-specific capacity, excellent rate capability and superior cycling performance. When evaluated as anode for SIBs at 0.3-3.0 V, the FeS_2 CF/3DGF electrode had high capacity stability than the FeS_2 FB/3DGF electrode, exploring a potential application in the next generation of SIBs.

Keywords: Cauliflower-like FeS_2; Graphene foam; Anode material; Sodium-ion batteries; Electrochemical performance.

1. INTRODUCTION

Rechargeable lithium-ion batteries have been successfully adopted and widely used in consumer electronics, electric vehicles, storage systems and other applications[1-5]. However, due to the limited lithium resources on Earth, researchers have been trying to explore alternative batteries. Recently, much effort has been devoted to sodium-ion batteries for their various advantages, such as high natural abundance, low cost and a greater probability of large-scale application [6-8]. Unfortunately, the larger ionic radius (1.02 Å) of sodium causes large volume change or serious collapse of electrode material structure during discharge-charge processes, especially under high current density [9-12]. Therefore, it is more challenging to find appropriate SIBs electrode materials [13,14].

Previously, metal sulfides have been widely studied as electrode materials because of their high theoretical capacities and chemical stability based on a conversion reaction mechanism [15-19]. According to sodium-ion storage, FeS_2 exhibits a high capacity of 894 $mAh \cdot g^{-1}$, but suffers serious volume expansion during oxidation-reduction processes [20-22]. Researchers have designed various

strategies to overcome the above-mentioned drawbacks to improve the industrial applications of FeS_2-based SIBs. A common and useful strategy entails restraining the discharge-charge voltage range (0.8-3.0 V) to control the adverse chemical reactions. For instance, Chen et al. reported FeS_2 microspheres that exhibited high-rate capability (170 $mAh \cdot g^{-1}$ at 20 $A \cdot g^{-1}$) and long capability with 90% capacity retention after 20000 cycles when tuning the cut-off voltage to 0.8 V [21,23]. However, the cycle stability improvement is achieved at the cost of the reversible capacity for the intercalation reaction. Coating FeS_2 with carbonaceous is another method that can accelerate the electron transfer, shorten ionic diffusion length and enhance the electrode structural stability. Also, FeS_2 materials with carbon from various sources have been developed to prepare FeS_2@C yolk-shell, which improved the electrical conductivity of FeS_2, showing excellent sodium storage performance [10, 24-26].

Herein, we propose the self-assembly of FeS_2 on a three-dimensional graphene foam (3DGF) with flower bud-like and cauliflower-like structures (labelled as FeS_2 FB/3DGF and FeS_2 CF/3DGF) by adjusting the preparation technology. The cauliflower-like FeS_2 based on 3D graphene foam improves structural stability and prevents structural collapse during charge-discharge processes. Furthermore, the cauliflower-like structure also reduces the electronic and ionic transmission, which benefits the electrochemical performance of SIBs.

2. EXPERIMENTAL

2.1 Synthesis of FeS_2 FB/3DGF and FeS_2 CF/3DGF

The 3DGF was obtained by chemical vapour deposition using nickel foam as a template. Other reagents were analytically pure and used without further treatment. 1 mmol of $FeCl_3.6H_2O$ and 0.25g of L-cysteine were mixed in 20 mL of D.I. water and stirred for 30 min to form a uniform solution. Next, 0.1 g sodium alkyl sulfate was added to the above mixture. The dispersion was transferred into a 50 mL Teflon stainless steel with a piece of 3DGF, which was sealed and maintained in a resistance furnace at 180 ℃ for 24 h. After cooling to room temperature, the obtained samples were washed with D.I. water and ethanol severally, followed by drying in a vacuum at 60 °C for 6 h. Thus, flower bud-like FeS_2 FB/3DGF was successfully prepared. The cauliflower-like FeS_2 CF/3DGF was obtained by annealing the above FeS_2 FB/3DGF at 500 ℃ under Ar for 4 h.

2.2 Material characterization

The phases and structures of the as-synthesized samples were characterized using X-ray diffraction (XRD) performed on Bruker D8 Advance (λ=0.15405 nm). The morphologies of the products were investigated using scanning electron microscopy (SEM JEOL JSM-6700F; JEOL, Tokyo, Japan) and transmission electron microscopy (TEM, JEOL-200CX) with an accelerating voltage of 200 kV.

2.3 Electrochemical measurements

Electrochemical measurements were measured using CR2032-type cells, which were assembled in a glove box under Ar. For the free-standing FeS_2 FB/3DGF and FeS_2 CF/3DGF anode materials, the cells were assembled without any binders. Glass fiber (Whatman) and sodium plate were used as the separator and counter electrode. Cyclic voltammetry measurements (0.3-3.0 V) and electrochemical impedance spectra (EIS) were measured from 0.01 to 100 kHz on a CHI660E electrochemical workstation (Shanghai, Chenhua). A Neware test system was used to measure cycling and rate performances.

3. RESULTS AND DISCUSSION

FeS_2 FB/3DGF and FeS_2 CF/3DGF were prepared first by a simple hydrothermal method and were subsequently annealed at 500 ℃. The preparation process was shown in Figure 1. Figure 1 showed that the 3D graphene foam, $FeCl_3.6H_2O$ and L-cysteine were dispersed in DI water. The FeS_2 FB/3DGF material was derived from the conventional hydrothermal reaction, and the cauliflower-like FeS_2 CF/3DGF was obtained by annealing at 500 ℃ under Ar for 4 h. The preparation details were described in the experimental section (Subsection 2.1). In comparison, the direct hydrothermal of FeS_2 FB/3DGF presented flower bud-like feature with much differences from the cauliflower-like feature of FeS_2 CF/3DGF. Notably, such morphology and structure change can improve electrical conductivity, as well as electron and ion transfer [3].

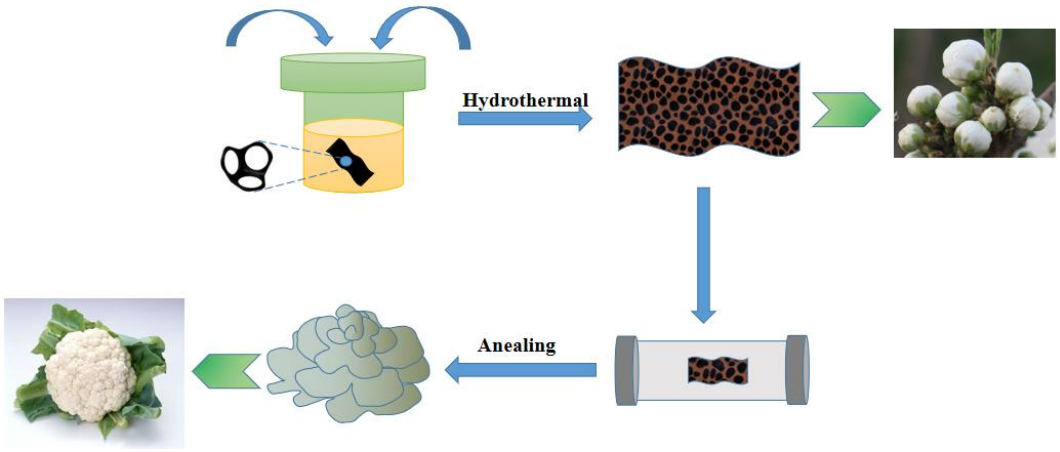

Figure 1. The typical synthesis process of FeS_2 FB/3DGF and FeS_2 CF/3DGF.

The morphologies and interior structures of FeS_2 FB/3DGF and FeS_2 CF/3DGF were characterized by SEM. Figure 2a indicated that FeS_2 FB/3DGF is evenly distributed on the surface of the 3DGF skeleton, which was generated from a one-step hydrothermal method. The higher magnification SEM images of FeS_2 FB/3DGF (Figure 2b) showed the flower bud-like features with little

holes as covered by a thin film. The diameters ranged from 1.0 to 5.0 μm. In comparison, FeS_2 CF/3DGF obviously showed cauliflower-like features (Figure 2c and Figure 2d) with few cracks. The cauliflower-like features of FeS_2 CF/3DGF connected with 3DGF network can not only restrain grown and volume expansion of FeS_2 during the sodiation or desodiation processes, but also provide effective electron and ionic transport pathway of 3DGF, which was beneficial for Na^+ insertion/deinsertion [27].

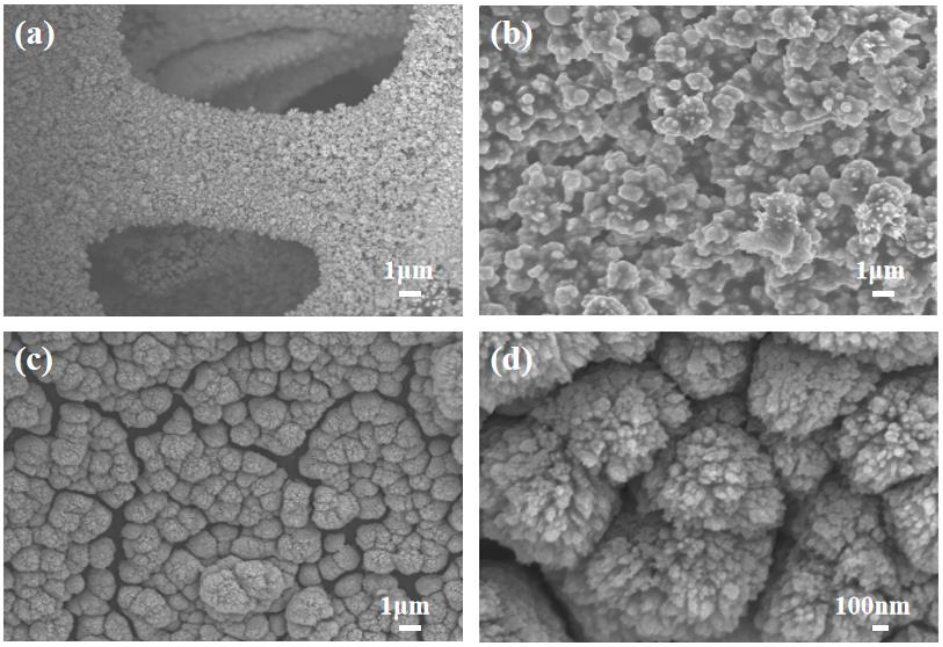

Figure 2. Morphology and structure of FeS_2 FB/3DGF and FeS_2 CF/3DGF (a) FeS_2 FB/3DGF (low resolution); (b) FeS_2 FB/3DGF (high resolution); (c) FeS_2 CF/3DGF (low resolution); (d) FeS_2 CF/3DGF (high resolution);

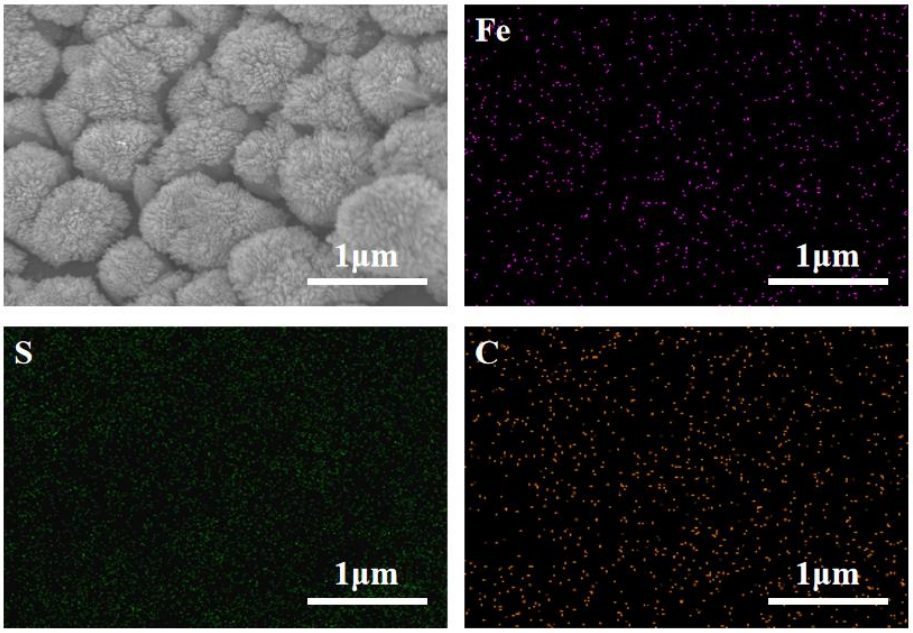

Figure 3. X-ray spectroscopy (EDS) elemental mapping images of Fe, S and C elements for FeS_2 CF/3DGF

To further clarify the distributions of Fe, S and C of FeS_2 CF/3DGF, elemental mappings were conducted using energy dispersive X-ray spectroscopy (Figure 3). The EDS results demonstrated that three elements of carbon, iron, and sulfur were uniformly distributed.

Furthermore, the structures of FeS_2 CF/3DGF were surveyed by examining the TEM images. Figure 4 showed that the structure of FeS_2 CF/3DGF was characterized by highly uniform nanorod morphology with an average of 40 nm width and 120 nm length, respectively.

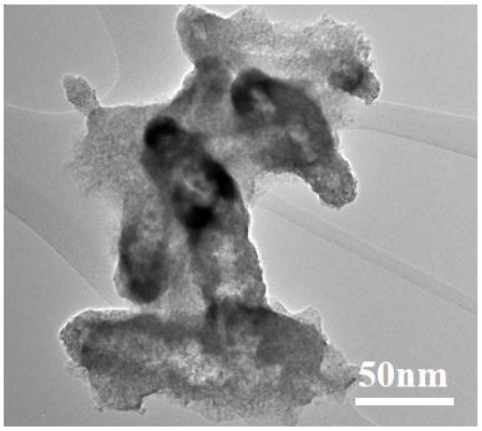

Figure 4. TEM images of FeS_2 CF/3DGF

Also, X-ray diffraction (XRD) was employed to further identify the crystal structures of the as-prepared FeS_2 FB/3DGF and FeS_2 CF/3DGF, as shown in Figure 5. For both of FeS_2 FB/3DGF and FeS_2 CF/3DGF, the diffraction peaks of FeS_2 (JCPDS card: 04-004-6512) indexed to the (111), (200), (210), (211), (220), and (311) lattice planes can be easily recognized [3,15]. Other peaks associated with graphene foam could be seen in the XRD patterns, indication high phase purity.

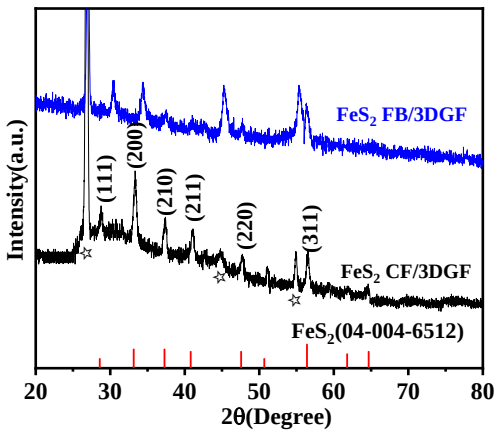

Figure 5. XRD patterns of FeS_2 FB/3DGF and FeS_2 CF/3DGF

To obtain the electrochemical performance of FeS_2 CF/3DGF electrodes, Figure 6 displayed the charge-discharge curves at a current density of 500 $mA \cdot g^{-1}$ for the first, second and third cycles. It should be emphasized that FeS_2 CF/3DGF possessed a smaller voltage polarization and larger capacity with no obvious capacity fading from the second cycle. The initial discharge and charge capacities of FeS_2 CF/3DGF were 589 $mAh \cdot g^{-1}$ and 502 $mAh \cdot g^{-1}$, respectively, corresponding to a coulombic efficiency (CE) of 85.2%. The initial capacity loss was mainly for electrolyte degradation which can be observed in other materials [28]. High CE of FeS_2 CF/3DGF may be ascribed to the uniform and defect-free 3D graphene form matrix. There was no significant capacity fading in the following desodiation/sodiation behaviors and the CE remained stable and higher than 97%, indicating the formation of an irreversible solid electrolyte interface (SEI) membrane on the electrode surface, which commonly indicated high capacity and well reversibility during charge-discharge process [12].

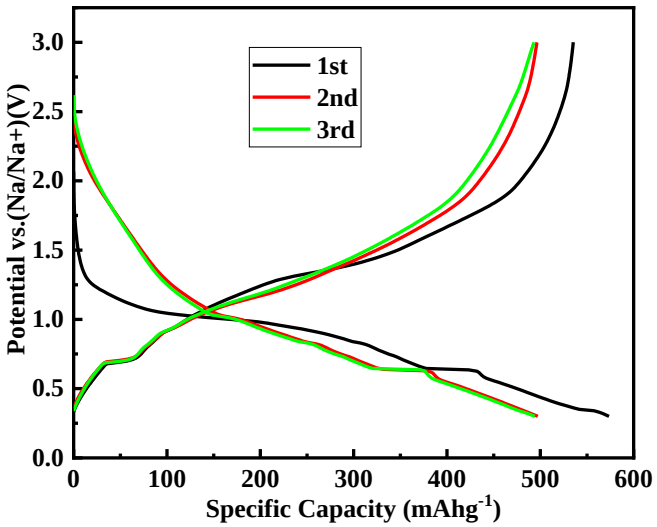

Figure 6. Galvanostatic discharge/charge voltage profiles for FeS_2 CF/3DGF at a current density of 500 $mA \cdot g^{-1}$

Besides, the rate performance of the FeS_2 FB/3DGF and FeS_2 CF/3DGF electrodes were characterized at different current densities and showed in Figure 7. As the current densities increased, the FeS_2 CF/3DGF displayed an average discharge capacity of 594 $mAh \cdot g^{-1}$, 461 $mAh \cdot g^{-1}$, 375 $mAh \cdot g^{-1}$, 214 $mAh \cdot g^{-1}$ and 205 $mAh \cdot g^{-1}$ at the current densities of 100 $mA \cdot g^{-1}$, 200 $mA \cdot g^{-1}$, 500 $mA \cdot g^{-1}$, 1 $mA \cdot g^{-1}$ and 2 $mA \cdot g^{-1}$, respectively. More importantly, when the current density decreased to 100 $mA \cdot g^{-1}$, the 550 $mAh \cdot g^{-1}$ capacity of FeS_2 CF/3DGF can be recovered, maintaining excellent rate reversibility under the same conditions. Notably, the capacity of FeS_2 CF/3DGF significantly exceeded that of FeS_2 FB/3DGF at different current densities, suggesting that the cauliflower-like features were indeed favourable for achieving high-rate performance [22].

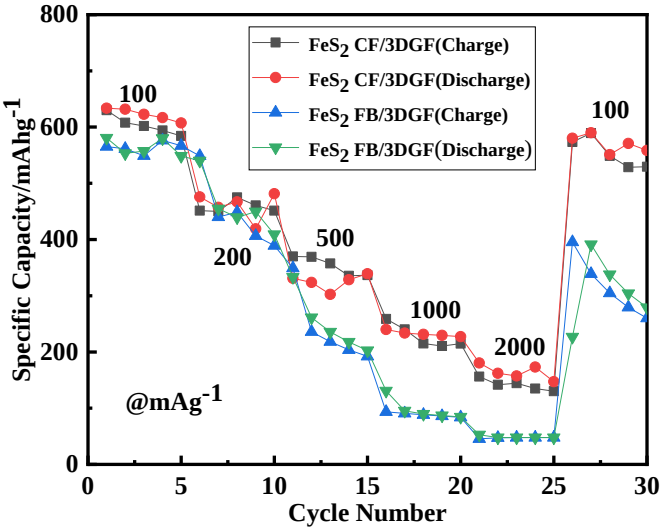

Figure 7. Rate capability of FeS_2 FB/3DGF and FeS_2 CF/3DGF at different current densities (100 $mA \cdot g^{-1}$-2000 $mA \cdot g^{-1}$)

Figure 8 showed the cycling performance of FeS_2 FB/3DGF and FeS_2 CF/3DGF at 500 $mA \cdot g^{-1}$. At the first cycle, the discharge and charge capacities of FeS_2 FB/3DGF were 445 $mAh \cdot g^{-1}$ and 424 $mAh \cdot g^{-1}$, respectively, and can maintain good cycling stability during the first cycles. Nevertheless, FeS_2 FB/3DGF suffered from rapid capacity decay during the next 50 cycles and maintained only 62% capacity after the 200th cycle, much lower than that of FeS_2 CF/3DGF (383 $mAh \cdot g^{-1}$). In contrast, the cycling performance of FeS_2 CF/3DGF was excellent with a reversible capacity of 408 $mAh \cdot g^{-1}$ at 100 cycles. The capacity decay in the first 20 cycles may be attributed to the activation process. Afterwards, nearly no degradation occurred for the next cycles with a coulomb efficiency close to 100%, further demonstrating superior cycling performance. This phenomenon was common in the iron-based anode material [12, 25].

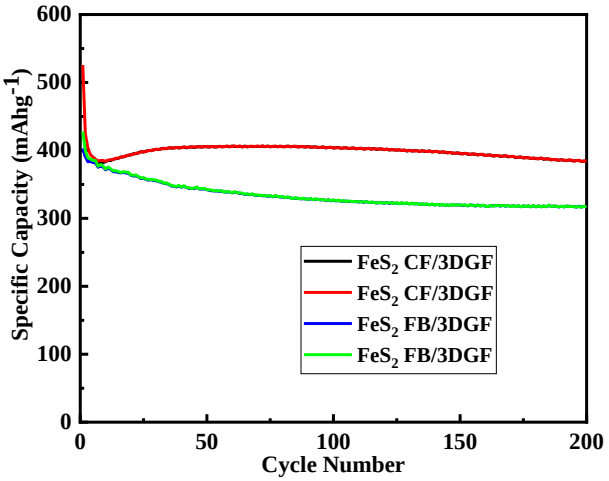

Figure 8. Cycling performance of FeS_2 FB/3DGF and FeS_2 CF/3DGF at a current of 500 $mA \cdot g^{-1}$

In addition, the electrochemical propertie of FeS_2 FB/3DGF and FeS_2 CF/3DGF were compared to those of previous studies in the literature. As can be seen from Table 1, the FeS_2 CF/3DGF with unique structure had better rate performance and higher specific capacity compared to other samples in the literature.

Table 1. Recent progress on electrochemical performance of FeS_2-based batteries

Materials	Voltage range(vs Na^+/Na)	Cycling	Rate capability	Ref.
FeS_2@rGO	0.8-3 V	252/250th/0.5 C	195/2 C	[29]
FeS2 NTs	0.01-3 V	358/50th/0.2 C	-	[15]
FeS2@C	0.01-3 V	265/200th/200 $mA\cdot g^{-1}$	197/2 $A\cdot g^{-1}$	[10]
pure FeS_2	0.01-3 V	200/70th/0.2 C	87/2 $A\cdot g^{-1}$	[30]
FeS_2 FB/3DGF	0.3 V-3.0 V	323/200th/500 $mA\cdot g^{-1}$	128/1 $A\cdot g^{-1}$	This paper
FeS_2 CF/3DGF	0.3 V-3.0 V	383/200th/500 $mA\cdot g^{-1}$	207/2 $A\cdot g^{-1}$	This paper

In order to understand the electrochemical kinetics and sodium-ion transfer performance of FeS_2 FB/3DGF and FeS_2 CF/3DGF, EIS measurements were carried out and shown in Figure 9. Clearly, the electrochemical impedance curves can be divided into three regions, such as, high frequency region, medium frequency region and low frequency region. The charge-transfer resistance of FeS2 CF/3DGF significantly exceeded that of FeS_2 FB/3DGF, as manifested by the smaller semicircle diameters in the middle-frequency region. Additionally, FeS_2 CF/3DGF also exhibited much lower Na-ion diffusion resistance, as indicated by the more inclined straight line in the low-frequency region, which is beneficial for facilitating the diffusion of electrolytes [3, 12-14].

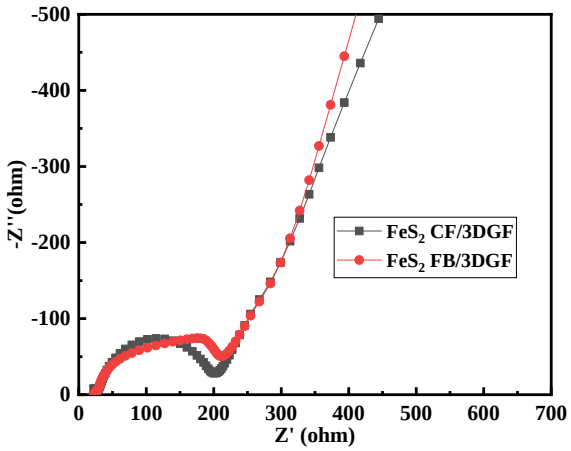

Figure 9. EIS plots of the FeS_2 FB/3DGF and FeS_2 CF/3DGF after 50 cycles.

4. CONCLUSION

In summary, free-standing flower bud-like FeS_2 FB/3DGF and cauliflower-like FeS_2 CF/3DGF were successfully synthesized from a simple solvothermal route and subsequently annealed. In the obtained samples, the uniform cauliflower-like feature provided enough space for electronic and ionic transport, and accommodated the volume change of active materials during charge-discharge processes. Consequently, the cauliflower-like FeS_2 CF/3DGF exhibited superior cycling stability (capacity retention of 408 $mAh \cdot g^{-1}$ after 200 cycles at 500 $mA \cdot g^{-1}$) and better rate capacity when used as anode materials for SIBs. Our findings opened a novel application by providing a simple strategy of morphology engineering.

References

1. W.J. Zhu, Y. Y. Wang, Y.Z. Yu, Y.H. Hu and Y.H. Chen, *J. Alloy Compd.*, 813 (2020) 152175.
2. Z.Y. Zhang, J.S. Liang, X. Zhang, W.F. Yang, X.L. Dong and Y.G Jung, *Int. J. Hydrogen Energy*, 45 (2020) 8186.
3. Wang L.Y., Liu, L.Q., Zhang C.C., Wang X. and Li X.Y., *Int. J. Electrochem. Sci.,* 16 (2021) 210643.
4. X.S. Yan, F.Y. Jiang, X.Q. Sun, R. D. and Y.L. Zhou, *J. Alloy Compd.*, 822 (2020) 153719.
5. C.T. Xue, Y. He, Y.J.Liu, P. Saha and Q.L. Cheng, *Ionics*, 25 (2019) 3069.
6. Z.Y. Chen, X. Wang, H.S. Wang, H. Wang, T. Bai, F. Ren, P.G. Ren, H.X. Yan, K.K. Xiao, Z.X. Shen, *J. Alloy Compd.*, 891 (2021) 161988.
7. L. Li, Y. Zheng, S.L. Zhang, J.P. Yang, Z.P. Shao and Z.P. Guo, *Energ Environ. Sci.*, 11 (2018) 2310.
8. H. Kang, Y. Liu, K. Cao, Y. Zhao, L. Jiao, Y. Wang and H. Yuan, *J. Mater. Chem. A*, 3 (2015) 17899.
9. Wang L.Y., Zhang Y.L., Li D.P., Wang X. and Li X.Y., *Int. J. Electrochem. Sci.,* 16 (2021) 211059.
10. L.Y. Yao, B.W. Wang, Y.C. Yang, X. Chen, J.H. Hu, D. Yang and A.G. Dong, *Chem. Commun.*, 55 (2019) 1229.
11. Y.X. Wang, W.H. Lai, Y.X. Wang, S.L. Chou, X.P. Ai, H.X. Yang and Y.L. Cao, *Angew. Chem. Int. Edit.*, 58 (2019) 18324.
12. F.B. Wang, G.D. Li, X.G. Meng, Y.X. Li, Q.F. Gao, Y.Q. Xu and W.F. Cui, *Inorg. Chem. Front.,* 5 (2018) 2462.
13. Y. Sun, S.H. Guo and H.S. Zhou, *Adv. Energy Mater.*, 9 (2019) 1.
14. L.P. Wang, L. Yu, X. Wang, M. Srinivasan and Z.J. Xu, *J. Mater. Chem. A*, 3 (2015) 9353.
15. L.B. Yao, W.W. Xia, H.T. Zhang, H. Dong, H.L. Xin, P. Gao, R.Cai, C.Y. Zhu, Y.Wu, M. Nie, S.Y. Lei, L.T. Sun and F. Xu, *Nano Energy*, 60 (2019) 424.
16. L.D. Shi, D.Z. Li, J.L. Yu, H.C. Liu, Y. Zhao, H.L. Xin, Y.M. Lin, C.D. Lin, C.H. Li and C.Z. Zhu, *J. Mater. Chem. A*, 6 (2018) 7967.
17. T. Wang, H.G. Yang and B.G. Lu*, J. Power Sources*, 399 (2018) 105.
18. Y.J. Zhang, W. Chang, J. Qu, S.M. Hao, Q.Y. Ji, Z.G. Jiang and Z.Z. Yu, *Chem. Eur. J.*, 24 (2018) 17339.
19. Z.W. Xu, T. Wang, L. Kong, K. Yao, H. Fu, K. Li, L.Y. Cao, J.F. Huang and Q.L. Zhang, *Adv. Sci.*, 34 (2017) 1600223.
20. L.Y. Wang, C.C. Zhang, L.Q. Liu and X. Wang, *J. Mater. Sci.: Mater. Electron.*, 32 (2021) 15665.
21. S.W. Wang, Y.P. Jing, L.F. Han, H. Wang, S.D. Wu, Y. Zhang, L.Z. Wang, K. Zhang, Y.M. Kang

and F.Y. Cheng, *Inorg. Chem. Front.*, 6 (2019) 459.
22. J.H. Lu, F. Lian, L.L. Guan, Y.X. Zhang and F.Ding, *J. Mater. Chem. A.*, 7 (2019) 991.
23. S.H. Qi, L.W. Mi, K.M. Song, K.W. Yang, J.M. Ma, X.M. Feng, J.M. Zhang and W.H. Chen, *J. Phys. Chem. C,* 123 (2019) 2775.
24. W.K. Ye, K. Wang, W.H. Yin, W.W. Chai and Y.H. Rui, *Electrochima. Acta,*323 (2019) 134817.
25. C.M. Chen, Y.C. Yang, X. Tang, R.H. Qiu, S.Y. Wang, G.Z. Cao and M. Zhang, *Small*, 15 (2019) 1804740.
26. M. Zhou, H.W. Tao, K.L. Wang, S.J. Cheng and K. Jiang, *J. Mater. Chem. A*, 6 (2018) 24425
27. Y.Sun, B. Fu, G.L. Yuan, M. Ma, H.Y. Jin, S.H. Xie and J.Y. Li, *Nanotechnology*, 31 (2020) 155401.
28. Z.C. Bai, Y.W. Zhang, Y.H. C.L. Guo and B.Tang, *Electrochima. Acta*, 159 (2015) 29.
29. W.H. Chen, S.H. Qi, M.M. Yu, X.M. Feng, S.Z. Cui, J.M. Zhang and L.W. Mi, *Electrochim. Acta*, 230 (2017) 1.
30. Q.F. Su, Y.H. Lu, S.H. Liu, X.C. Zhang, Y.H. Lin, R.W. Fu and D.C. Wu, *Carbon*, 140 (2018) 433